BOUNDARY LAYER FLOW AND HEAT TRANSFER OF CROSS FLUID OVER A STRETCHING SHEET

Masood KHAN, Mehwish MANZUR[1] and Masood ur RAHMAN

Department of Mathematics, Quaid-i-Azam University, Islamabad 44000, Pakistan.

Abstract: The current study is a pioneering work in presenting the boundary layer equations for the two-dimensional flow and heat transfer of the Cross fluid over a linearly stretching sheet. The system of partial differential equations is turned down into highly non-linear ordinary differential equations by applying suitable similarity transformations. The stretching sheet solutions are presented via. a numerical technique namely the shooting method and graphs are constructed. The impact of the emerging parameters namely the power-law index n, the local Weissenberg number We and the Prandtl number $\Pr$ on the velocity and temperature fields are investigated through graphs. The numerical values of the local skin friction coefficient and the local Nusselt number are also presented in tabular form. Additionally, the graphs are sketched for the local skin friction coefficient and the local Nusselt number. It is observed that with growing values of the local Weissenberg number We, the velocity profiles exhibited a decreasing trend while opposite behavior is seen for the temperature field. Further, comparisons are made with previously available literature for some limiting cases and an excellent agreement is achieved.
Keywords: Cross fluid; Stretching sheet; Heat Transfer; Numerical solution.

1. Introduction

Nowadays, the generalized Newtonian fluids have gained massive prominence amongst researchers on account of their significant practicality in industrial, chemical and technological mechanisms. In the generalized Newtonian fluids [1-2] the viscosity is shear dependent as a result of which a new constitutive relation is defined by making modifications in the Newton's law of viscosity to account for the change in viscosity with varying shear rate. The most common type of the generalized Newtonian fluids is the power-law fluid [3] which tenders a simplest representation of the shear-thinning/thickening behaviors of several fluids. Despite of the abundant process engineering applications, the main limitation of the power-law fluid is that it cannot describe the fluid behavior for very low and very high shear rates but only for limited range of shear rate called the power-law region. When the deviation from the power-law model is notable only at very low shear rate, Ellis model [4] is utilized. Likewise, Sisko model [5] characterize the flow of fluids in the power-law and very high shear rate region. In order to overcome all the limitations of the above mentioned rheological models, a broader sub-class of the generalized Newtonian fluids namely the Cross model was introduced by Cross [6]. This model is competent of depicting the flow in the power-law region as well as the regions of very low and very high shear rates. Unlike the power-law fluid, we achieve a finite viscosity as the shear rate gets zero $(\dot{\gamma} = 0)$ and secondly it involves a time constant due to which it is good enough for many engineering calculations. Examples of the applications of the Cross model includes the synthesis of the polymeric solutions like 0.35% aqueous solution of Xanthan gum, blood, aqueous solution of polymer latex sphere, 0.4% aqueous solution of polyacrylamide [7]. The Cross rheology equation [8-9] for viscosity in terms of shear rate is given as:

[1]Corresponding author. E-mail address: mehwish.manzur@gmail.com

$$\eta^* = \eta_\infty + (\eta_0 - \eta_\infty)\left[\frac{1}{1+(\Gamma\dot{\gamma})^n}\right], \tag{1}$$

or equivalently,

$$\frac{\eta_0 - \eta^*}{\eta^* - \eta_\infty} = (\Gamma\dot{\gamma})^n, \tag{2}$$

where η_0 and η_∞ are the limiting viscosities at low and high shear rates, respectively. Γ is the material Cross time constant, n the dimensionless constant, commonly known as the flow behavior index and $\dot{\gamma} = \sqrt{\left(\frac{1}{2}\Pi\right)}$ the shear rate with Π the second invariant strain rate tensor. Cross [6] presented an experimental data for many systems by using a simple value $n = 2/3$ but he clearly stated that there is no hindrance in treating n as an adjustable parameter [10]. This model predicts the usual Newtonian fluid if $\Gamma = 0$.

It is interesting to note that by making certain approximation to the Cross equation, we can achieve various other popular viscosity models like the power-law model, the Sisko model and the Bingham model. When $\eta^* << \eta_0$ and $\eta^* >> \eta_\infty$, the Cross equation (2) reduces to

$$\eta^* = K_1/(\dot{\gamma})^n, \tag{3}$$

which is the well-known power-law model with K_1 the consistency index and n the power-law index.

Furthermore, if $\eta^* << \eta_0$, we get

$$\eta^* = \eta_\infty + K_1/(\dot{\gamma})^n, \tag{4}$$

which is the renowned Sisko rheological model.

Further, by setting $n = 0$ in Sisko model and by slight redefinition of parameters we attain

$$\eta^* = \mu_B + \sigma_0\dot{\gamma}, \tag{5}$$

which represents the Bingham model [11] such that μ_B is the Bingham plastic viscosity and σ_0 is the Bingham yield stress.

In the past two decades experimental based study is done on the Cross model by several investigators. Escudier *et al*. [12] performed the experimental analysis and presented the fluid-flow data by fitting the Cross model to the non-Newtonian liquid particularly the Xanthan gum (XG). Xie and Jin [13] investigated the Cross rheology equation to analyze the free surface flow of non-Newtonian fluids. For the numerical implementation of the Cross equation, the WC-MPS method was employed to determine the four rheology parameters of the Cross model.

The analysis of the flow and heat transfer over a continuously stretching surface has acquired great importance due to its occurring in many engineering and industrial applications like drawing of rubber and plastic sheets, polymer processing and metallurgy, crystal growing, food processing and many others. The rate of cooling and stretching renders significant part in controlling the quality of the final product. The boundary layer flow over a moving surface with constant speed was initiated by Sakiadis [14]. Later, Crane [15] extended this work for the case of linearly stretching sheet. After these pioneering attempts, research on the flow and heat transfer over a stretching surface has immensely been done by various investigators [16-19].

A thorough survey of the literature reveals that the Cross fluid which predicts the pseudoplastic nature of the fluid over a wide range of shear rate has not been given due attention. In fact to the best of authors knowledge no attempt has been made on the boundary layer flow and heat transfer of the Cross fluid. The present work fills this gap by presenting the boundary layer equations for the flow of Cross fluid over a linearly stretching sheet. The governing equations are numerically solved by the help of the shooting technique and effect of the pertinent parameters is revealed through graphs and tables.

2. Governing equations

The conservation equations of mass, linear momentum and energy for the flow of an incompressible fluid are

$$\operatorname{div}\mathbf{V}=0, \tag{6}$$

$$\rho\frac{d\mathbf{V}}{dt}=\operatorname{div}\boldsymbol{\tau}, \tag{7}$$

$$\rho c_p\frac{dT}{dt}=\boldsymbol{\tau}.\mathbf{L}-\operatorname{div}\mathbf{q}, \tag{8}$$

where $\mathbf{V}$ symbolizes the velocity vector, ρ the density, $\boldsymbol{\tau}$ the Cauchy stress tensor, T the fluid temperature, c_p the specific heat at constant pressure, $\mathbf{q}\left(=-k\nabla T\right)$ the heat flux vector, $\mathbf{L}=\nabla\mathbf{V}$ and $\frac{d}{dt}$ the material derivative.

The Cauchy stress tensor for the four parameter fluid is defined as

$$\boldsymbol{\tau}=-p\mathbf{I}+\eta^{*}\mathbf{A}_1, \tag{9}$$

where η^{*} for the Cross fluid is given by Eq. (1), where

$$\mathbf{A}_1=\mathbf{L}+\mathbf{L}^{T},\ \Pi=tr\left(\mathbf{A}_1^{2}\right), \tag{10}$$

such that p is the pressure, $\mathbf{I}$ denotes the identity tensor and $\mathbf{A}_1$ the first Rivlin-Ericksen tensor.

The infinite shear rate viscosity η_{∞} is frequently set equal to zero [20-22] in Eq. (1) and accordingly Eq. (9) reduces to

$$\boldsymbol{\tau}=-p\mathbf{I}+\eta_0\left[\frac{1}{1+\left(\Gamma\dot{\gamma}\right)^{n}}\right]\mathbf{A}_1. \tag{11}$$

The salient feature of the Cross model is that when $0<n<1$ the fluid is shear-thinning. Additionally, this model reduces to the usual Newtonian fluid when $\Gamma\to 0$.

For a two-dimensional flow in Cartesian coordinates, we assume the velocity and temperature fields of the form

$$\mathbf{V}=\left[u\left(x,y\right),v\left(x,y\right),0\right],\ T=T\left(x,y\right), \tag{12}$$

where u and v are the $x-$ and $y-$components of the velocity vector.

Keeping in view Eq. (12), the shear rate $\dot{\gamma}$ is expressed as:

$$\dot{\gamma}=\left[4\left(\frac{\partial u}{\partial x}\right)^{2}+\left(\frac{\partial u}{\partial y}+\frac{\partial v}{\partial x}\right)^{2}\right]^{\frac{1}{2}}. \tag{13}$$

Substituting Eq. (12) in Eqs.(6) and (7), bearing in mind Eqs. (11) and (13), a straight forward calculation yields the following governing equations

$$\frac{\partial u}{\partial x}+\frac{\partial v}{\partial y}=0, \tag{14}$$

$$\rho\left(u\frac{\partial u}{\partial x}+v\frac{\partial u}{\partial y}\right)=-\frac{\partial p}{\partial x}+2\eta_0\frac{\partial}{\partial x}\left[\frac{\frac{\partial u}{\partial x}}{1+\left\{\Gamma^2\left(4\left(\frac{\partial u}{\partial x}\right)^2+\left(\frac{\partial u}{\partial y}+\frac{\partial v}{\partial x}\right)^2\right)\right\}^{\frac{n}{2}}}\right]$$
$$+\eta_0\frac{\partial}{\partial y}\left[\frac{\left(\frac{\partial u}{\partial y}+\frac{\partial v}{\partial x}\right)}{1+\left\{\Gamma^2\left(4\left(\frac{\partial u}{\partial x}\right)^2+\left(\frac{\partial u}{\partial y}+\frac{\partial v}{\partial x}\right)^2\right)\right\}^{\frac{n}{2}}}\right], \tag{15}$$

$$\rho\left(u\frac{\partial v}{\partial x}+v\frac{\partial v}{\partial y}\right)=-\frac{\partial p}{\partial y}+\eta_0\frac{\partial}{\partial x}\left[\frac{\left(\frac{\partial u}{\partial y}+\frac{\partial v}{\partial x}\right)}{1+\left\{\Gamma^2\left(4\left(\frac{\partial u}{\partial x}\right)^2+\left(\frac{\partial u}{\partial y}+\frac{\partial v}{\partial x}\right)^2\right)\right\}^{\frac{n}{2}}}\right]$$
$$+2\eta_0\frac{\partial}{\partial y}\left[\frac{\frac{\partial v}{\partial y}}{1+\left\{\Gamma^2\left(4\left(\frac{\partial u}{\partial x}\right)^2+\left(\frac{\partial u}{\partial y}+\frac{\partial v}{\partial x}\right)^2\right)\right\}^{\frac{n}{2}}}\right], \tag{16}$$

The above equations of motion are made non-dimensional through the following relations

$$(x,y)=L(x^*,y^*),(u,v)=U(u^*,v^*)\text{ and }p=\rho U^2p^*. \tag{17}$$

In terms of the dimensionless variables, the continuity and momentum equations take the following forms:

$$\frac{\partial u^*}{\partial x^*}+\frac{\partial v^*}{\partial y^*}=0, \tag{18}$$

$$u^*\frac{\partial u^*}{\partial x^*}+v^*\frac{\partial u^*}{\partial y^*}=-\frac{\partial p^*}{\partial x^*}+2\varepsilon_1\frac{\partial}{\partial x^*}\left[\frac{\frac{\partial u^*}{\partial x^*}}{1+\left\{\varepsilon_2\left(4\left(\frac{\partial u^*}{\partial x^*}\right)^2+\left(\frac{\partial u^*}{\partial y^*}+\frac{\partial v^*}{\partial x^*}\right)^2\right)\right\}^{\frac{n}{2}}}\right]$$
$$+\varepsilon_1\frac{\partial}{\partial y^*}\left[\frac{\left(\frac{\partial u^*}{\partial y^*}+\frac{\partial v^*}{\partial x^*}\right)}{1+\left\{\varepsilon_2\left(4\left(\frac{\partial u^*}{\partial x^*}\right)^2+\left(\frac{\partial u^*}{\partial y^*}+\frac{\partial v^*}{\partial x^*}\right)^2\right)\right\}^{\frac{n}{2}}}\right], \tag{19}$$

$$u^*\frac{\partial v^*}{\partial x^*}+v^*\frac{\partial v^*}{\partial y^*}=-\frac{\partial p^*}{\partial y^*}+\varepsilon_1\frac{\partial}{\partial x^*}\left[\frac{\left(\frac{\partial u^*}{\partial y^*}+\frac{\partial v^*}{\partial x^*}\right)}{1+\left\{\varepsilon_2\left(4\left(\frac{\partial u^*}{\partial x^*}\right)^2+\left(\frac{\partial u^*}{\partial y^*}+\frac{\partial v^*}{\partial x^*}\right)^2\right)\right\}^{\frac{n}{2}}}\right]$$
$$+2\varepsilon_1\frac{\partial}{\partial y^*}\left[\frac{\frac{\partial v^*}{\partial y^*}}{1+\left\{\varepsilon_2\left(4\left(\frac{\partial u^*}{\partial x^*}\right)^2+\left(\frac{\partial u^*}{\partial y^*}+\frac{\partial v^*}{\partial x^*}\right)^2\right)\right\}^{\frac{n}{2}}}\right], \tag{20}$$

where the dimensionless parameters are defined as:

$$\varepsilon_1=\frac{\frac{\eta_0}{\rho}}{LU}\text{ and }\varepsilon_2=\frac{\Gamma^2}{\left(\frac{L}{U}\right)^2}. \tag{21}$$

Using the standard boundary layer assumptions, where x, u, p are of order 1 while v and y are of order δ. The dimensionless parameters ε_1 and ε_2 are of order δ^2.

Keeping in view the boundary layer analysis, one finally has the following equations in dimensional form

$$\frac{\partial u}{\partial x}+\frac{\partial v}{\partial y}=0, \tag{22}$$

$$u\frac{\partial u}{\partial x}+v\frac{\partial u}{\partial y}=-\frac{1}{\rho}\frac{\partial p}{\partial x}+\nu\frac{\partial}{\partial y}\left[\frac{\frac{\partial u}{\partial y}}{1+\left\{\Gamma\left(\frac{\partial u}{\partial y}\right)\right\}^{n}}\right], \tag{23}$$

where $\nu=\frac{\eta_0}{\rho}$ gives the kinematic viscosity.

3. Problem formulation

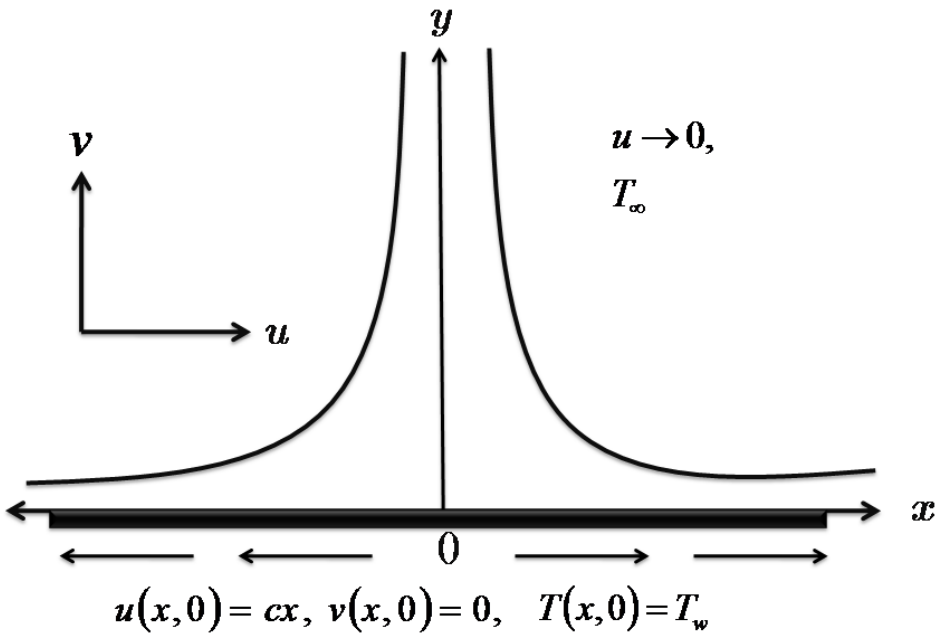

Figure 1: Geometry of the problem.

The steady two-dimensional flow and heat transfer of an incompressible generalized Newtonian fluid specifically the Cross fluid is considered by incorporating the effects of stretching surface. The stretching sheet is taken to be coinciding with the plane $y=0$ while the fluid occupies the region $y>0$ (as shown in figure 1). The sheet is uniformly stretched along the $x-$axis with a velocity $U=cx,$ where $c\,(>0)$ is the stretching rate of the sheet. We assume that the temperature near the surface of the sheet is T_w while T_∞ is the ambient fluid temperature. Moreover, for the present case the driving pressure gradient is not present and the flow is driven only due to stretching sheet.

Under these assumptions, the system of equations governing the flow and heat transfer is

$$\frac{\partial u}{\partial x}+\frac{\partial v}{\partial y}=0, \tag{24}$$

$$u\frac{\partial u}{\partial x}+v\frac{\partial u}{\partial y}=\nu\frac{\partial}{\partial y}\left[\frac{\frac{\partial u}{\partial y}}{1+\left\{\Gamma\left(\frac{\partial u}{\partial y}\right)\right\}^{n}}\right], \tag{25}$$

$$u\frac{\partial T}{\partial x}+v\frac{\partial T}{\partial y}=\alpha\frac{\partial^2 T}{\partial y^2}, \tag{26}$$

where $\alpha\left(=\frac{k}{\rho c_p}\right)$ is the thermal diffusivity and k being the thermal conductivity and c_p the specific heat at constant pressure.

The relevant boundary conditions of the problem under consideration are:

$$u(x,y)=U(x)=cx,\ v(x,y)=0,\ T(x,y)=T_w \quad \text{at } y=0, \tag{27}$$

$$u(x,y)\to 0,\ T(x,y)\to T_\infty \quad \text{as } y\to\infty. \tag{28}$$

Employing the following local similarity transformations

$$\eta=\sqrt{\frac{c}{\nu}}y,\ \ \psi=\sqrt{\nu c}xf(\eta),\ \ \theta(\eta)=\frac{T-T_\infty}{T_w-T_\infty}, \tag{29}$$

where η denotes the dimensionless local similarity variable and ψ the stream function such that $(u,v)=\left(\frac{\partial\psi}{\partial y},-\frac{\partial\psi}{\partial x}\right)$. In consideration of the above transformations, the incompressibility condition (24) is automatically satisfied while Eqs. (25-28) are reduced to

$$\left[ff''-(f')^2\right]\left[1+(Wef'')^n\right]^2+\left[1+(1-n)(Wef'')^n\right]f'''=0, \tag{30}$$

$$\theta''+\Pr f\theta'=0, \tag{31}$$

$$f(\eta)=0,\ f'(\eta)=1,\ \theta(\eta)=1 \quad \text{at } \eta=0, \tag{32}$$

$$f'(\eta)\to 0,\ \theta(\eta)\to 0 \quad \text{as } \eta\to\infty, \tag{33}$$

where prime denotes differentiation with respect to η, We stands for the local Weissenberg number and $\Pr$ the Prandtl number defined as:

$$We=c\Gamma\,\mathrm{Re}^{\frac{1}{2}},\ \ \Pr=\frac{\eta_0 c_p}{k}, \tag{34}$$

such that $\mathrm{Re}\left(=\frac{cx^2}{\nu}\right)$gives the local Reynolds number.

The boundary layer equations for the flow and heat transfer of Newtonian fluid can be achieved by setting $We=0$ in Eqs. (30-33).

The expression for the local skin friction coefficient and the local Nusselt number is given by

$$C_f=\frac{\tau_w}{\frac{1}{2}\rho U^2},\quad N_u=\frac{xq_w}{k(T_w-T_\infty)}, \tag{35}$$

where τ_w signifies the local wall shear stress and q_w the surface heat flux defined as:

$$\tau_w=\tau_{xy}\big|_{y=0}=\left[\eta_0\frac{\frac{\partial u}{\partial y}}{1+\left\{\Gamma\left(\frac{\partial u}{\partial y}\right)\right\}^{1-n}}\right]_{y=0},\ q_w=-k\frac{\partial T}{\partial y}\bigg|_{y=0}. \tag{36}$$

In view of Eq. (29), the dimensionless forms of the local skin friction coefficient and the local Nusselt number can be obtained as

$$\frac{1}{2}\mathrm{Re}^{\frac{1}{2}} C_{f_x} = \frac{f''(0)}{1+\left(Wef''(0)\right)^{1-n}}, \quad -\mathrm{Re}^{-\frac{1}{2}} Nu_x = \theta'(0). \tag{37}$$

4. Results and discussion

The non-linear differential equations (30) and (31) subject to boundary conditions (32) and (33) are numerically solved by the help of shooting method. The influence of the emerging parameters is graphically examined and discussed in this section. The authenticity of the obtained numerical results is verified by making comparison with the existing literature. The numerical values of the local skin friction coefficient and the local Nusselt number are also tabulated.

The impact of the power-law index n on the velocity and temperature fields is respectively shown in figures 2 and 3. An analysis of figure 2 shows that the incremented values of n enlarges the fluid velocity for shear-thinning fluid $(n<1)$. Figure 3 discloses that a decline in the temperature field is seen for shear-thinning regime. Furthermore, the momentum boundary layer thickness increases for growing values of power-law index while thermal boundary layers thickness shows a diminishing trend. The physical reason behind this trend is that shear-thinning fluid renders less resistance to fluid motion due to less viscosity and due to which the velocity profile increases and the fluid temperature decreases.

Figures 4 and 5 are sketched to demonstrate the behavior of the velocity and temperature profiles corresponding to a change in local Weissenberg number We. Figure 4 exhibits that the velocity profiles as well as the momentum boundary layer thickness are lowered by increasing the Weissenberg number. An elevation in the temperature and the thermal boundary layer is noticed for growing values of We as displayed in figure 5. From the physical point of view, an increase in We causes an enlargement in the relaxation time which results in lowering the fluid velocity and escalating the fluid temperature.

Figure 6 is plotted to see the dependence of the temperature profile on the Prandtl number. The growing values of the Prandtl number results in the reduction of the temperature distribution and thermal boundary layer thickness. Physically, the Prandtl number demonstrates the ratio of the momentum diffusivity to thermal diffusivity. For elevated values of Pr, the thermal diffusivity gets weaker as a result the flow of heat into the fluid is restrained and thermal boundary layer structures gets diminished. Heat diffuses faster from the wall for the fluids having low Prandtl number due to high thermal conductivity. Thus, Prandtl number acts as a controlling factor in conducting flows for monitoring the rate of cooling.

The effect of the power-law index n and the local Weissenberg number We on the local skin friction coefficient and the local Nusselt number are revealed by figures 7 and 8, respectively. It is visualized that the local skin friction coefficient and the local Nusselt number show opposite trend for growing values of the power-law index. Figure 7 reveals that the local skin friction coefficient is lowered by increasing the power-law index as well as the local Weissenberg number. Figure 8 demonstrates that the local Nusselt number is a growing function of the power- law index n while a decreasing function of the local Weissenberg number We.

In order to authenticate the present results a comparative study is made with the existing results in the literature. Table 1 is constructed to provide comparison of the value of $-f''(0)$ with the results of Cortell [26], Cortell [27] and Hamad and Ferdows [28] for the case of viscous fluid. A comparison with the work of Wang [29], Gorla and Sidawi [30] and Hamad [31] is given in Table 2. The numerical values of the local Nusselt number is calculated for the limiting case $(We=0)$. An excellent compatibility with the existing literature is thus acheived.

The numerical values of the local skin friction coefficient and the local Nusselt number are tabulated in tables 3 and 4, respectively. The consequence of the power-law index n and the local Weissenberg number We on the local skin friction coefficient is displayed in Table 3. It is inferred from the data that the

magnitude of the skin friction coefficient is a decreasing function of the Weissenberg number for fixed value of n. Further, it is seen that the magnitude of the local skin friction coefficient is lowered for growing values of n. The influence of the power-law index n, local Weissenberg number We and the Prandtl number $\Pr$ on the local Nusselt number is provided in Table 4 by presenting numerical data. It is deduced that the local Nusselt number enlarges with augmenting values of the Prandtl number $\Pr$. This is due to the fact that the growing values of $\Pr$ enhances the process of convection in comparison with the conduction due to which the rate of heat transfer increases. Opposite trend is revealed for the case of growing values of the local Weissenberg number We. It is also noticed that the rate of heat transfer is enhanced with a rise in the values of the power-law index n.

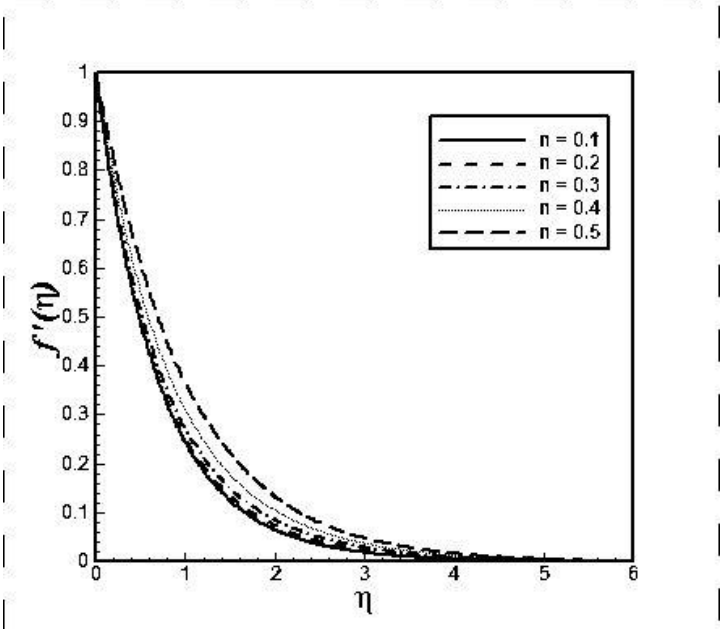

Figure 2: Velocity profiles for different values of the power law index n when $We = 2$.

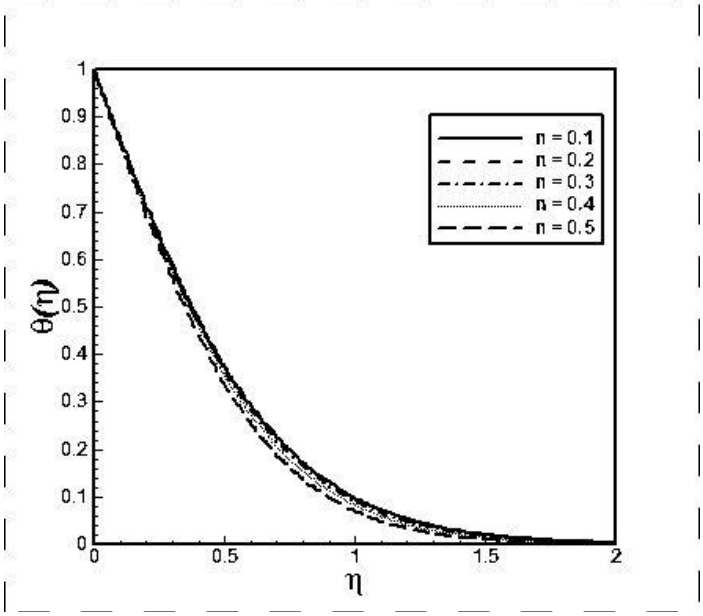

Figure 3: Temperature profiles for different values of the power law index n when $We = 2$ and $\Pr = 5$.

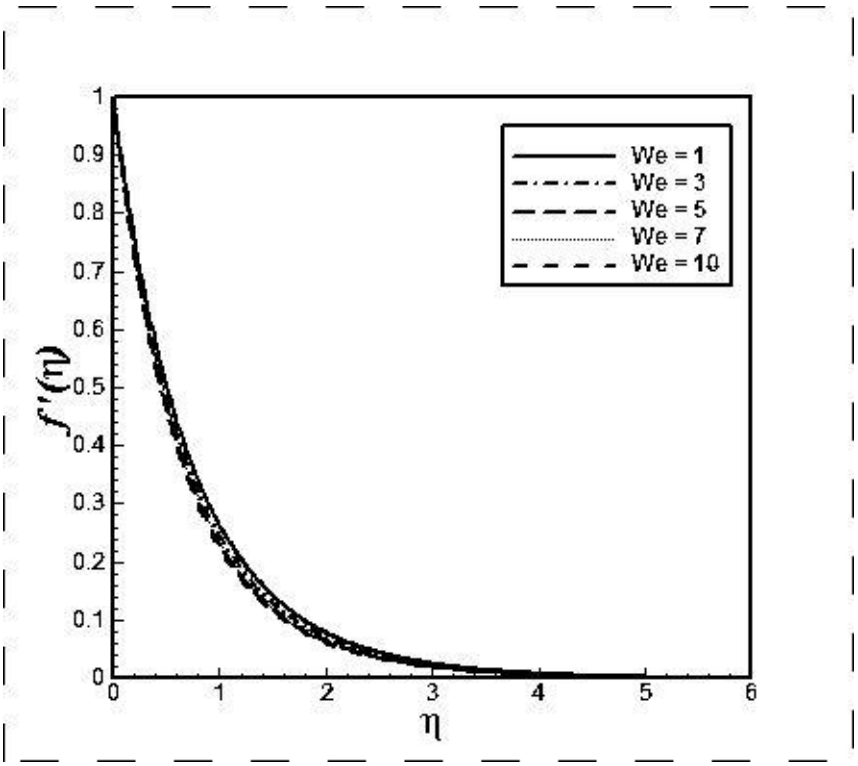

Figure 4: Velocity profiles for different values of the local Weissenberg number We **when** $n = 0.2$.

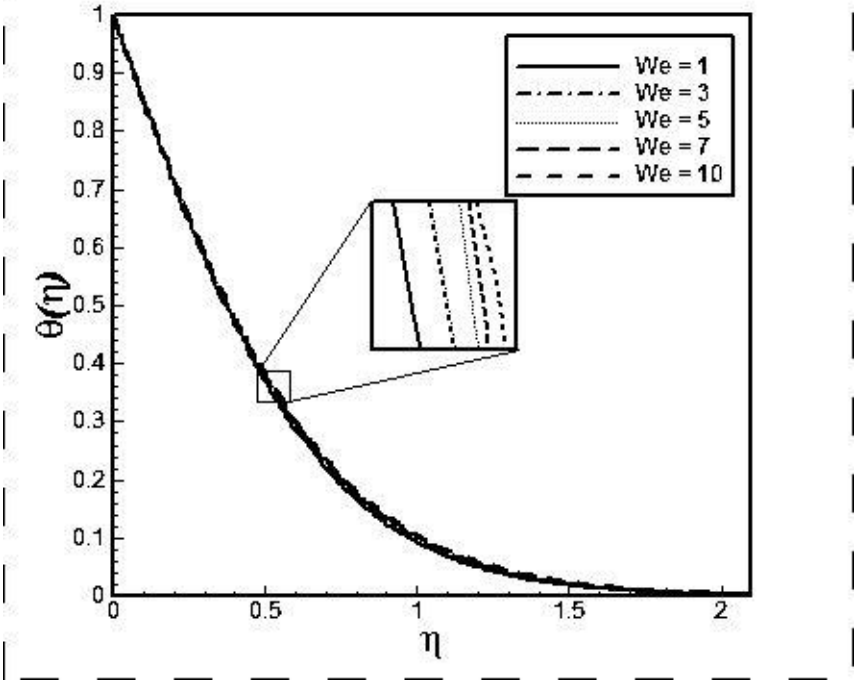

Figure 5: Temperature profiles for different values of the local Weissenberg number We **when** $n = 0.2$ **and** $\Pr = 5$.

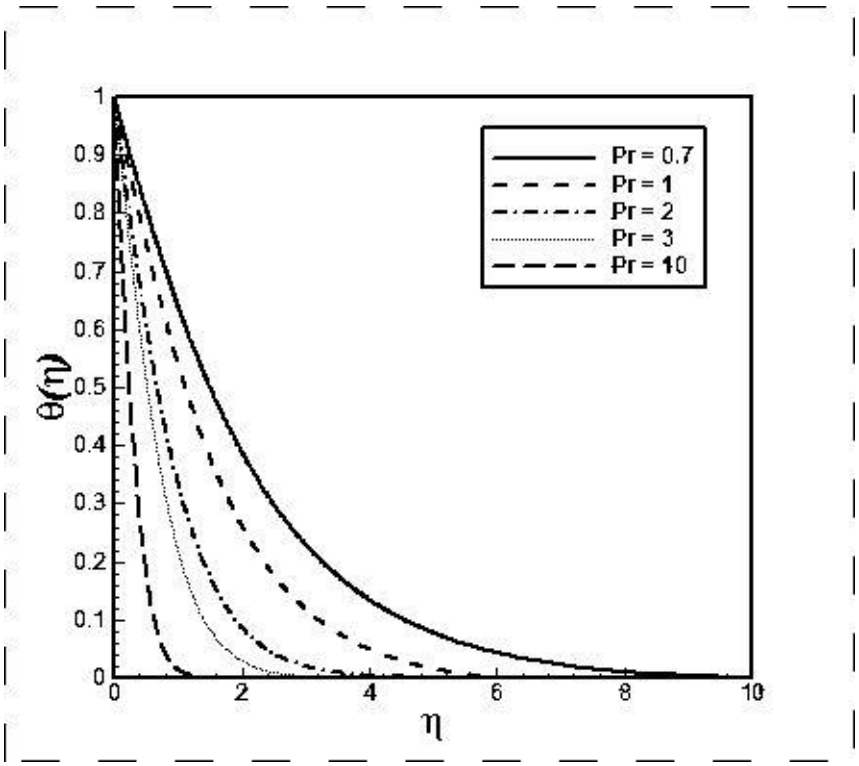

Figure 6: Temperature profiles for different values of the Prandtl number Pr **when** $We = 2$ **and** $n = 0.2$.

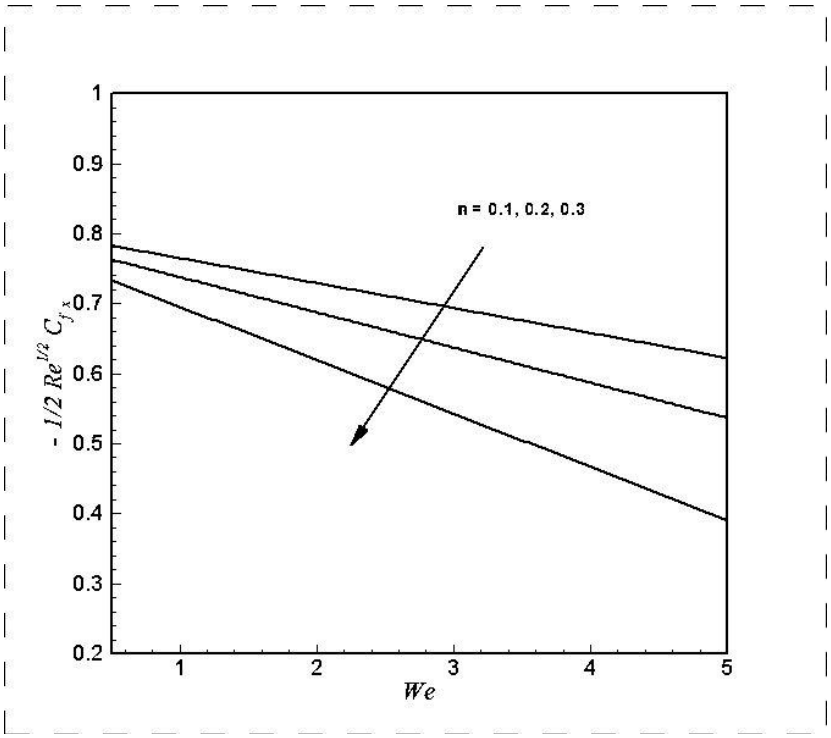

Figure 7: The local skin friction coefficient for different values of the power-law index n **and local Weissenberg number** *We.*

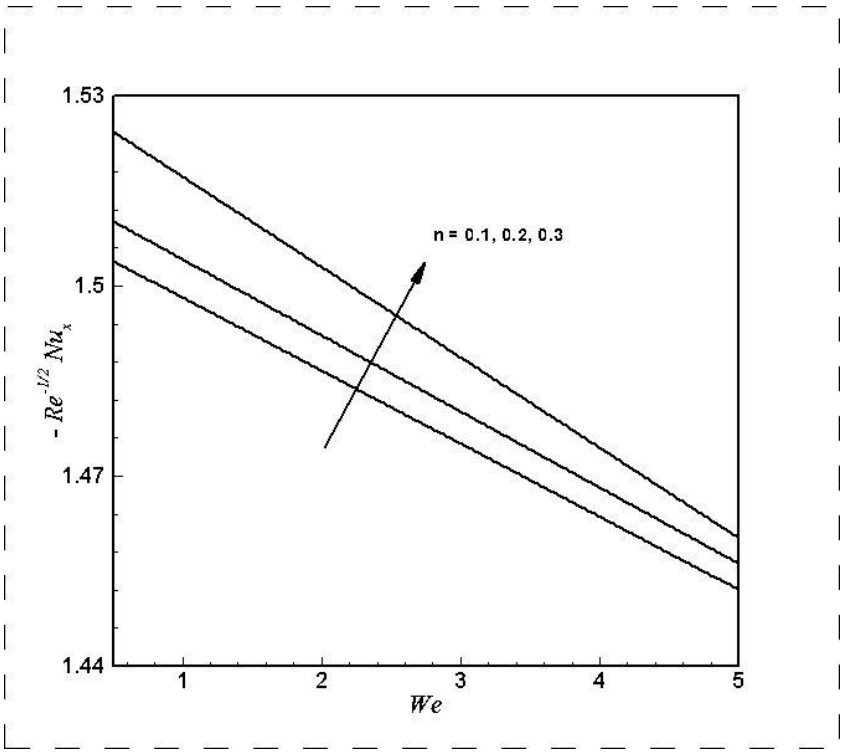

Figure 8: The local Nusselt number for different values of the power-law index n and local Weissenberg number We when $\Pr = 5$.

Table 1: Comparison of the values of $-f''(0)$ for the case of the Newtonian fluid $(We = 0)$.

	Cortell [26]	Cortell [27]	Hamad and Ferdows [28]	Present result
$-f''(0)$	1.0	1.0	1.0043	1.00001

Table 2: **Comparison of the variation of $-\theta'(0)$ for the Newtonian fluid $(We = 0)$.**

Pr	$-\theta'(0)$			
	Wang [29]	Gorla and Sidawi [30]	Hamad [31]	Present results $(We = 0)$
0.07	0.0656	0.0656	0.0656	0.065526
0.2	0.1691	0.1691	0.1691	0.164037
0.7	0.4539	0.4539	0.4539	0.418299
2	0.9114	0.9114	0.9114	0.826827
7	1.8954	1.8905	1.8954	1.80433
20	3.3539	3.3539	3.3539	3.25603
70	6.4622	6.4622	6.4622	6.36662

Table 3: **Numerical values of the local skin friction coefficient** $\left(-\frac{1}{2}\mathrm{Re}^{\frac{1}{2}}C_f\right)$ **for various values of** We **and** n.

Parameters (fixed values)	Parameters		$-\frac{1}{2}\mathrm{Re}^{\frac{1}{2}}C_f$
$We=2$	n	0.1	0.684867
		0.2	0.635007
		0.3	0.549867
		0.4	0.433523
		0.5	0.318336
$n=0.2$	We	1	0.661872
		2	0.635007
		3	0.615357
		4	0.601791
		5	0.589208

Table 4: **Numerical values of the local Nusselt number** $\left(-\mathrm{Re}^{\frac{1}{2}}Nu_x\right)$ **for various values of** We, n **and** Pr.

Parameters (fixed values)	Parameters		$-\mathrm{Re}^{\frac{1}{2}}Nu_x$
$We=2,\ \mathrm{Pr}=5$	n	0.1	1.473410
		0.2	1.477390
		0.3	1.493460
		0.4	1.525000
		0.5	1.572540
$n=0.2,\ \mathrm{Pr}=5$	We	1	1.488060
		2	1.477390
		3	1.470620
		4	1.465500
		5	1.459620
$n=0.2,\ We=2,$	Pr	0.7	0.407252
		1	0.515167
		2	0.827280
		3	1.077400
		4	1.289770

5. Concluding remarks

The present study is an inaugural work in bestowing the boundary layer equations for the flow of the Cross fluid. The modelled partial differential equations were converted to ordinary differential equations by the help of suitable local similarity transformations and then numerically integrated by employing the shooting technique. The graphs were constructed for the velocity and temperature fields corresponding to the emerging parameters. The main findings are summarized as:

- The uplifting values of the power-law index in the shear- thinning regime $(n<1)$, boosted the momentum boundary layer thickness while a decline in the thermal boundary layer was observed.
- A decline in the velocity profile was visualized for growing values of the local Weissenberg number. However, the temperature profiles exhibited a progressive trend.
- The escalated values of the Prandtl number lessened the temperature profile as well as the thermal boundary layer thickness.
- It was seen that the magnitude of the local skin friction coefficient and the local Nusselt number decreased for growing values of the local Weissenberg number.

Acknowledgement: This work has the financial support of the Higher Education Commission (HEC) of Pakistan.

6. References

[1] Bird, R.B., Curtiss, C.F., Armstrong, R.C.,Hassager, O., Dynamics of Polymeric Liquids, Wiley, New York, 1987
[2] Bird, R.B., Useful non-Newtonian models, Annual Review of Fluid Mechanics, 8 (1976), pp. 13-34
[3] Hassanien, I.A., Abdullah, A.A., Gorla, R.S.R., Flow and heat transfer in a power-law fluid over a non-isothermal stretching sheet, Mathematical and Computer Modelling, 28 (1998), pp. 105-116
[4] Matsuhisa, S., Bird, R.B., Analytical and numerical solutions for laminar flow of the non-Newtonian Ellis fluid, American Institute of Chemical Engineers Journal, 11 (1965), pp. 588-595
[5] Sisko, A.W., The flow of lubricating greases, Industrial and Engineering Chemistry, 50 (1958), pp. 1789-1792
[6] Cross, M.M., Rheology of non-Newtonian fluids: A new flow equation for pseudoplastic systems, Journal of Colloid Science, 20 (1965), pp. 417-437
[7] Barnes, H.A., Hutton, J.F.,Walters, K., An Introduction to Rheology, Elsevier Science, Amsterdam, 1989
[8] Rao, M.A., Rheology of Fluid, Semisolid, and Solid Foods, Springer, New York, 2014
[9] Steffe, J.F., Rheological Methods in Food Process Engineering, Freeman, USA, 1992
[10] Gan, Y.X., Continuum Mechanics-Progress in Fundamentals and Engineering Applications, InTech, China, 2012
[11] Bingham, E.C., Fluidity and Plasticity, McGraw-Hill, New York, 1922
[12] Escudier, M.P., et al., On the reproductivity of the rheology of shear-thinning liquids, Journal of Non-Newtonian Fluid Mechanics, 97 (2001), pp. 99-124
[13] Xie, J., Jin, Y.C., Parameter determination for the Cross rheology equation and its application to modeling non-Newtonian flows using the WC-MPS method, Engineering Applications of Computational Fluid Mechanics, 10 (2015), pp. 111-129
[14] Sakiadis, B.C., Boundary layer behavior on continuous solid surfaces, American Institute of Chemical Engineers Journal, 7 (1961), pp. 26-28
[15] Crane, L.J., Flow past a stretching sheet, Zeit Angew Math. Phys., 21 (1970), pp. 645-647
[16] Andersson, H.I., Bech, K.H., Magnetohydrodynamic flow of a power-law fluid over a stretching sheet, International Journal of Non-Linear Mechanics, 27 (1992), pp. 929-936

[17] Howell, T.G., Jeng, D.R., Witt, K.J.D., Momentum and heat transfer on a continuous moving surface in a power law fluid, Journal of Heat and Mass Transfer, 40 (1997), pp. 1853-1861
[18] Khan, M., Rahman, M., Flow and heat transfer to modified second grade fluid over a non-linear stretching sheet, AIP Advances, 5 (2015), 087157
[19] Myers, T.G., Application of non-Newtonian models to thin film flow, Physical Review, 72 (2005), 066302
[20] Mabood, F., Khan, W.A., Analytical study for unsteady nanofluid MHD flow impinging on heated stretching sheet, Journal of Molecular Liquid, 219 (2016), 216-223
[21] Mabood. F., Ibrahim. S.M., Khan. W.A., Framing the features of Brownian motion and thermophoresis on radiative nanofluid flow past a rotating stretching sheet with magnetohydrodynamics, Results in Physics, 6 (2016), 1015-1023
[22] Mabood. F., Ibrahim. S.M., Rashidi. M.M., Shadloo. M.S., Lorenzini. G., Non-uniform heat source/sink and Soret effects on MHD non-Darcian convective flow past a stretching sheet in a micropolar fluid with radiation, International Journal of Heat and Mass transfer, 93 (2016), 674-682
[23] Rahman. M.U., Manzur. M., Khan. M., Mixed convection heat transfer to modified second grade fluid in the presence of thermal radiation, Journal of Molecular Liquids, 223 (2016), 217-223
[24] Khan. M., Rahman. M.U., Manzur. M., Axisymmetric flow and heat transfer to modified second grade fluid over a radially stretching sheet, Results in Physics, 7 (2017), 878-889
[25] Osswald. T.A., Rudolph, N., Polymer Rheology: Fundamentals and Applications, Hanser, 2014
[26] Cortell, R., Viscous flow and heat transfer over a nonlinearly stretching sheet, Applied Mathematics and Computation, 184 (2007), pp. 864-873
[27] Cortell, R., Effects of viscous dissipation and radiation on the thermal boundary layer over a non-linearly stretching sheet, Physics Letter, A 372 (2008), pp. 631-636
[28] Hamad, M.A.A., Ferdows, M., Similarity solutions to viscous flow and heat transfer of nanofluid over nonlinearly stretching sheet, Applied Mathematics and Mechanics English, 33 (2012), pp. 923-930
[29] Wang, C.Y., Free convection on a vertical stretching surface, Journal of Applied Mathematics and Mechanics (ZAMM), 69 (1989), pp. 418-420
[30] Gorla, R.S.R., Sidawi, I., Free convection on a vertical stretching surface with suction and blowing, Applied Science Research, 52 (1994), pp. 247-257
[31] Hamad, M.A.A., Analytical solution of natural convection flow of a nanofluid over a linearly stretching sheet in the presence of magnetic field, International Communications inHeat and Mass Transfer, 38 (2011), pp. 487-492